Supplementary methods and figures

for

Combined near infrared photoacoustic imaging and ultrasound detects vulnerable atherosclerotic plaque

Martin Karl Schneider[1]*, James Wang[1]*, Aris Kare[1], Shaunak S. Adkar[2], Darren Salmi[3], Caitlin F. Bell[2], Tom Alsaigh[2], Dhananjay Wagh[4], John Coller[4], Aaron Mayer[5], Sarah J. Snyder[6], Alexander Borowsky[7], Steven R. Long[8], Maarten G. Lansberg[9], Gary K. Steinberg[10], Jeremy J. Heit[6], Nicholas J. Leeper[2], Katherine W. Ferrara[1]

*authors contributed equally

[1] Molecular Imaging Program at Stanford and Bio-X Program, Department of Radiology, Stanford University School of Medicine, Palo Alto, CA 94305, USA

[2] Department of Surgery, Division of Vascular Surgery, Stanford University School of Medicine, Stanford, CA 94305, USA.

[3] Department of Pathology, Stanford University School of Medicine, Palo Alto, CA 94305, USA

[4] Sequencing Group Stanford Genomics, Stanford University School of Medicine, Palo Alto, CA 94305, USA

[5] Enable Medicine, Menlo Park, CA, 94025, USA

[6] Department of Radiology and Neurosurgery, Stanford University School of Medicine, Palo Alto, CA 94305, USA

[7] Department of Pathology and Laboratory Medicine, UC Davis Medical Center, Davis, CA 95616, USA

[8]Department of Pathology, University of California San Francisco, San Francisco, CA 94110, USA

[9] Department of Neurology and Neurological Sciences, Stanford University School of Medicine, Palo Alto, CA 94305, USA

[10] Department of Neurosurgery, Stanford University School of Medicine, Palo Alto, CA 94305, USA

List of contents:

Supplementary Methods

Near-infrared auto-photoacoustic (NIRAPA) imaging

The lateral resolution of the Vevo LAZR-X imaging system with a 15-MHz (10–22 MHz) linear-array transducer was 100 µm, which also corresponds to the lateral spatial resolution of the transcriptomic data. In order to reduce ultrasound reflections, the human carotid plaque was placed on fixed gauze in a custom-made polyvinyl chloride plastisol vial (Item No. 8228SS, M-F Manufacturing Company). 0.35% intralipid (CAS Number: 68890-65-3, Sigma-Aldrich) was dissolved in phosphate buffered saline (PBS) to simulate tissue-specific light scattering properties.

Immunohistochemistry

Five-µm tissue sections were stained with hematoxylin and eosin (H&E), Masson's trichrome (Sigma Aldrich) and picrosirius red (24901; Polysciences, USA). Picrosirius red sections were imaged using polarized light (AxioImager Widefield Fluorescence Microscope, Zeiss).

After the plaques were fixed in 4% paraformaldehyde (PFA) and paraffin embedded, 5-µm slices were sectioned from the tissue block. Paraffin was removed using Xylene and then hydrated deploying an alcohol/water gradient. The de-paraffinized slides were air dried and imaged for the NIRAF signal using a digital slide scanner (CY5, Olympus VS120, exposure time 500 ms, 20x objective). The staining protocol was continued by antigen retrieval in citrate buffer (cat. no.: C9999, Sigma-Aldrich, USA) for 20 min at 95 degrees Celsius. After the slides reached room temperature, they were washed using a wash buffer (PBS + 0.1% Tween) and subsequently treated with 3% hydrogen peroxide for 10 min to block endogenous peroxidase activity. Following an additional washing step in wash buffer, the sections were incubated with goat serum (Vector Laboratories, CA, USA) for 30 min. The sections were then covered with a primary antibody and incubated overnight at 4 degrees Celsius. Anti-CD68 (clone KP1, BioLegend, USA, dilution 1:250), anti-alpha-SMA (cat no: ab5694, Abcam, USA, dilution 1:200) and anti-bilirubin (clone 24G7, Shino-test, Kanagawa, Japan, dilution 1:200) were used as primary antibodies. After washing off the primary antibody, the sections were incubated with a corresponding biotinylated secondary antibody for 30 min at room temperature. Following an additional washing step, the sections were incubated with a DAB (3, 3'-diaminobenzidine) substrate kit for peroxidase detection (Vector Laboratories). No counterstaining was performed to achieve maximal contrast for digital imaging processing.

Cluster annotation

The macrophage cluster was isolated and further sub-clustered with a resolution value of 0.8, 20 k-nearest neighbors, and a Jaccard index cutoff of 0.005. The macrophage cluster was annotated based on the expression of *CD68*, *CD14*, *HLA-DRB1*, *HLA-DRA*, and *APOE*. The *ACTA2*$^{+}$ myofibroblast cluster was based on the expression of *ACTA2*, *COL1A1*, *COL1A2*, and *CNN2*. Pro-inflammatory macrophages were defined by the higher expression of *CD74, HLA-DRA,* and *APOE*[1]. Foamy macrophages were defined by the higher expression of *CTSB*, *TREM1*, *S100A10,* and *SPP1*[1]. A cluster, with combined weak expression of *COL1A1*, *COL3A1*, *CD68*, *CD14* and *SPP1,* was categorized as smooth muscle cell (SMC) derived intermediate cell types[2].

Enrichment analysis

Spatial sequencing results from vulnerable and stable plaques were combined, and their differential expression genes were determined by comparing the fold change of mean expression across the genes based on a negative binomial distribution. Genes with a fold change > 0, denoting upregulation, were selected and enriched with the gene ontology biological process database[3].

Transcriptomic correlation with NIR

To prepare spatial transcriptomics outputs for signal correlation with NIR, we first plotted gene expression levels in gray scale. Subsequently, we isolated the spatial spots as an image and performed a circular median filtering process with a filter diameter of 15 pixels. The image intensities were then normalized based on minimum to maximum normalization. Regions of interest across the plaque were selected for key genes and the Pearson's correlation for expression and image intensities was calculated and plotted.

Supplementary Figures and Tables

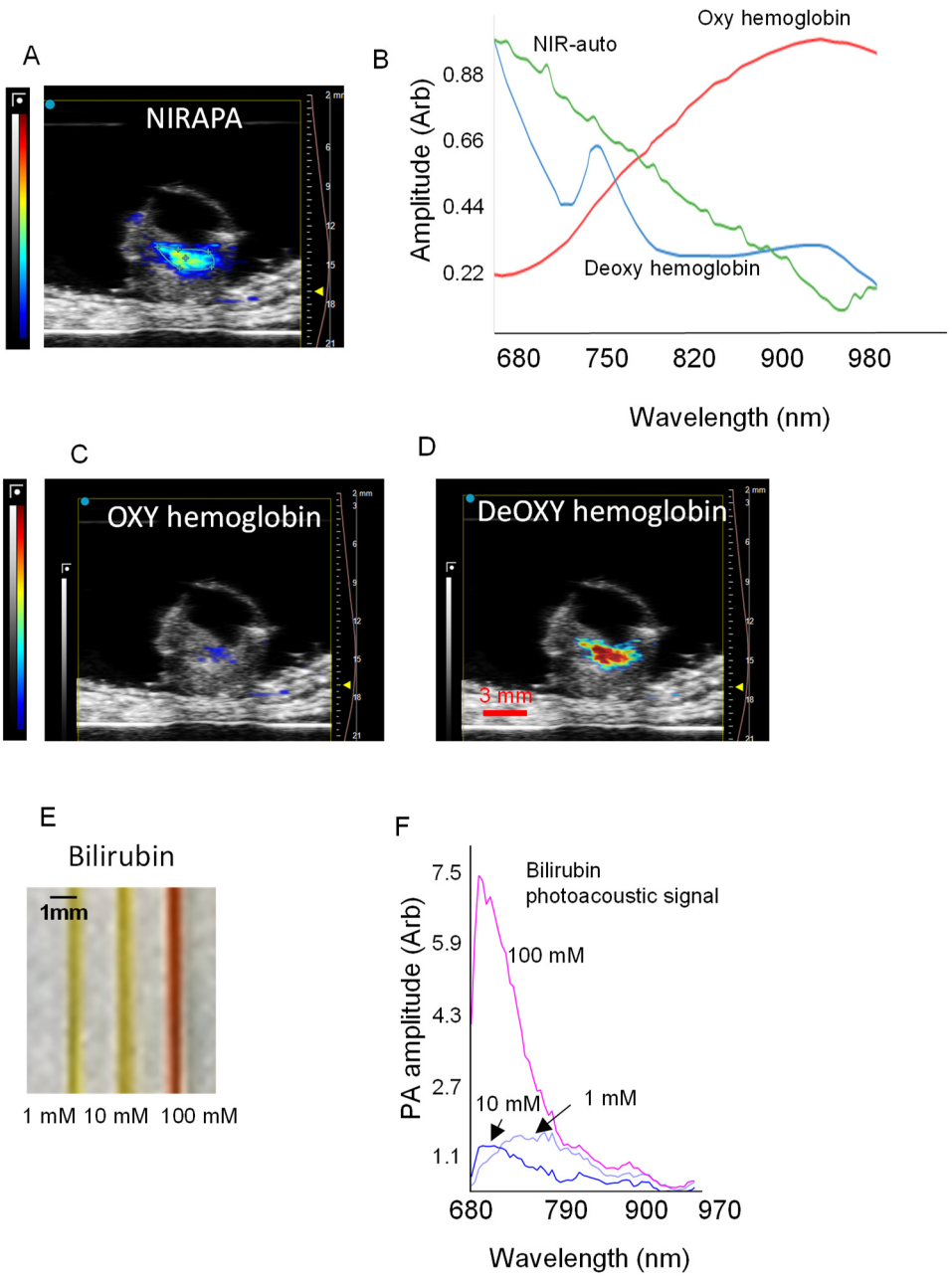

Supplementary Fig. 1. Spectrum of the NIRAPA signal and the bilirubin correlation. A) Near-infrared auto-photoacoustic (NIRAPA) sample image. B) Spectra of NIRAPA (NIR-auto) and Vevo unmixing into spectra for oxyhemoglobin (HbO_2) and deoxyhemoglobin (Hb). C-D) Spectrally unmixed images of C) Oxyhemoglobin (HbO_2), D) Deoxyhemoglobin (Hb) calculated by Vevo. E) Photoacoustic phantom containing 1 mM, 10 mM and 100 mM of bilirubin in dimethyl sulfoxide (DMSO). F) Photoacoustic (PA) signal spectra of different bilirubin concentrations.

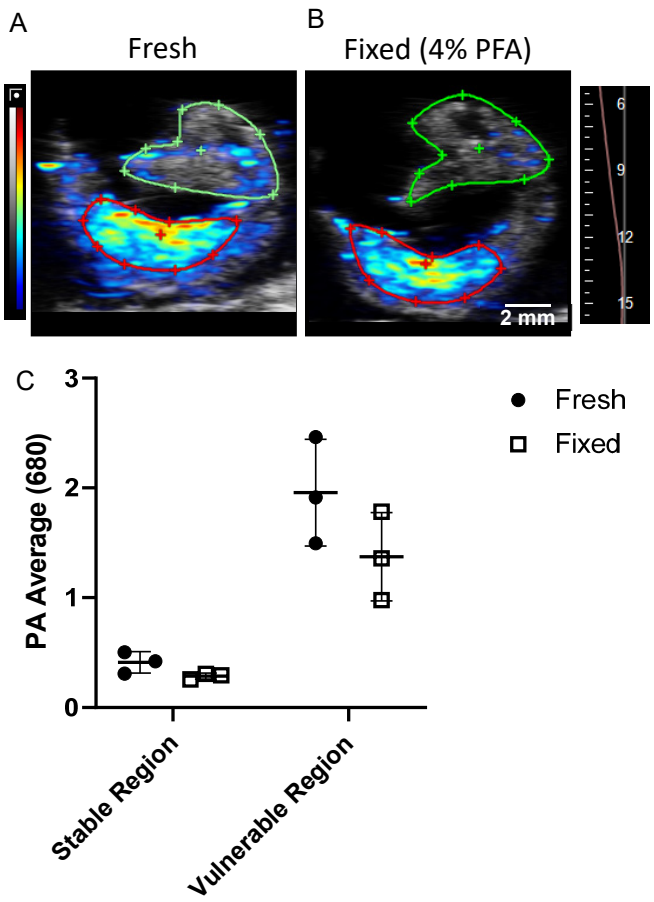

Supplementary Fig. 2. Comparing NIRAPA signal in fresh and 4% PFA fixed carotid plaque tissue. A) Fresh/unfixed plaque tissue showing the NIRAPA signal in stable (green) and vulnerable (red) plaque areas. B) Same plaque tissue, but fixed with 4% PFA. NIRAPA signal intensity in stable (green) and vulnerable (red) plaque areas. C) NIRAPA signal intensity results (PA Average (680)) in stable and vulnerable plaque regions acquired from 3 representative images of a 3D longitudinal plaque scan.

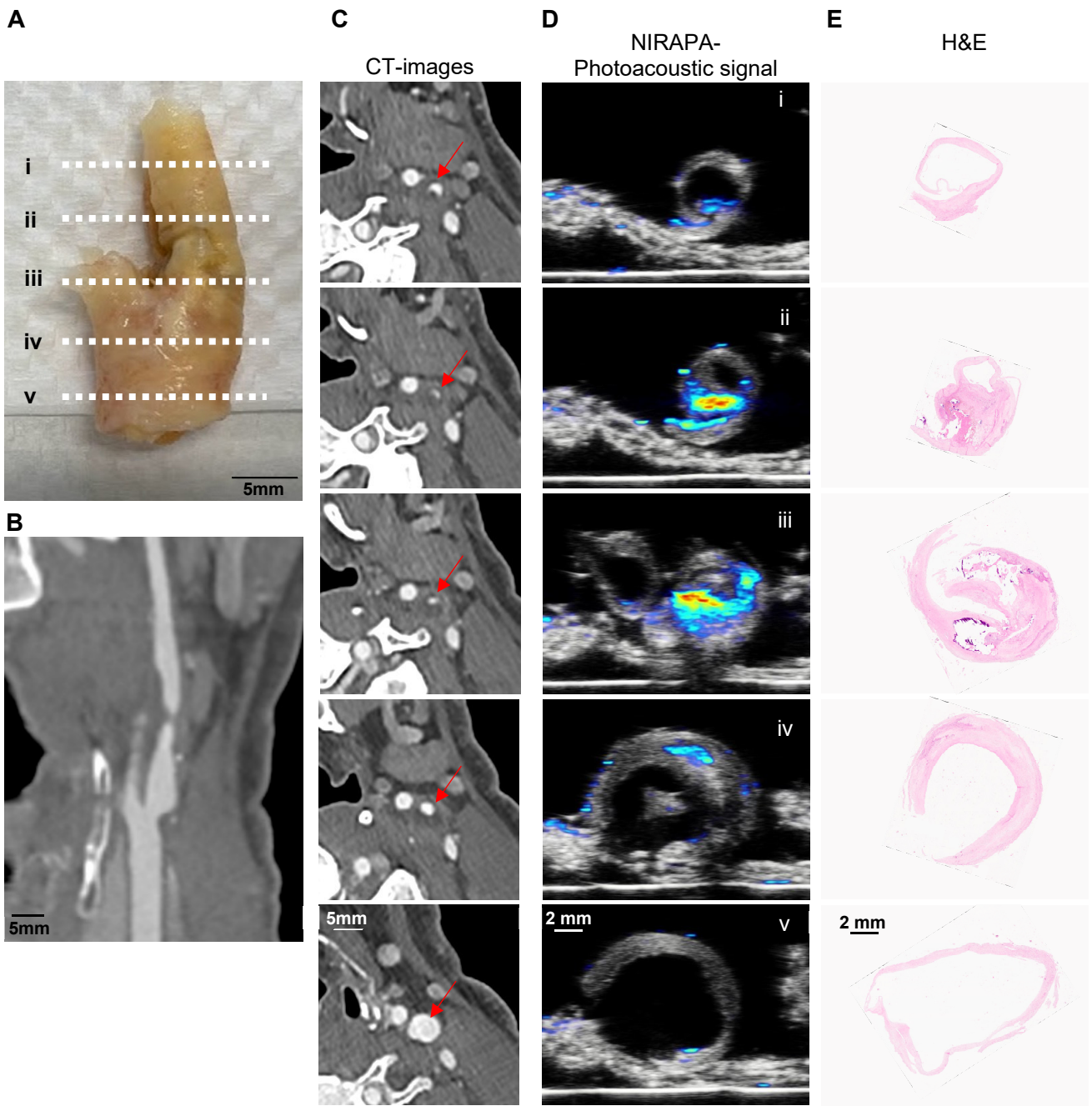

Supplementary Fig. 3. Comparison of contrast CT images with PAI images using the NIRAPA signal to detect vulnerable plaque composition of a stable carotid artery. A) Human carotid endarterectomy (CEA) specimen under white light. B) Corresponding longitudinal contrast computed tomography (CT) image shown underneath. The dashed lines on the longitudinal image represent the imaging locations of the axial images in columns C-E. C) Serial axial CT sections through the lesion of the carotid artery with locations of the stenosis shown by red arrows. D) Serial axial PAI sections through the lesion of the carotid artery showing the NIRAPA signal. E) Corresponding H&E stains.

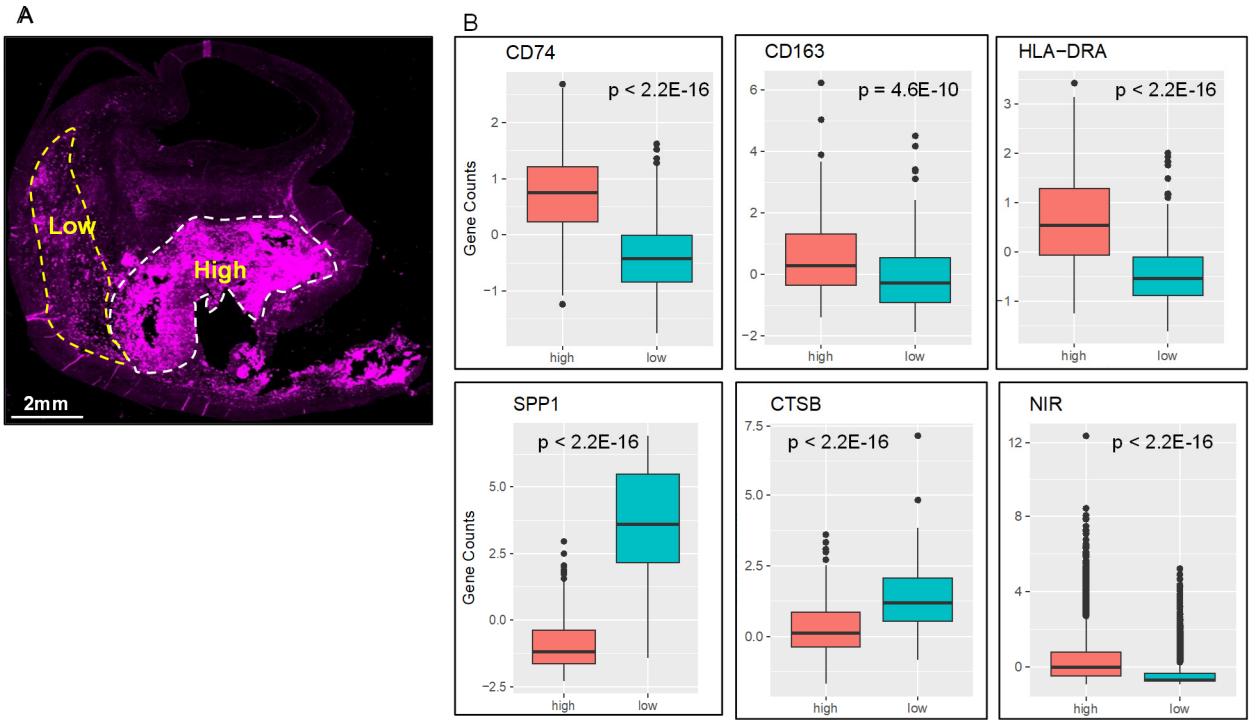

Supplementary Fig. 4. Quantification and statistical comparison of the key gene counts corresponding to NIRAF signal regions based on Visium spatial transcriptomics with the high and low regions determined by NIRAF microscopic imaging. A) Plaque regions with high and low NIRAF signal and B) *CD74*, *CD163*, *HLA-DRA*, *SPP1*, *CTSB* and NIRAF (NIR) signal level comparison between high and low signal regions and their p-values.

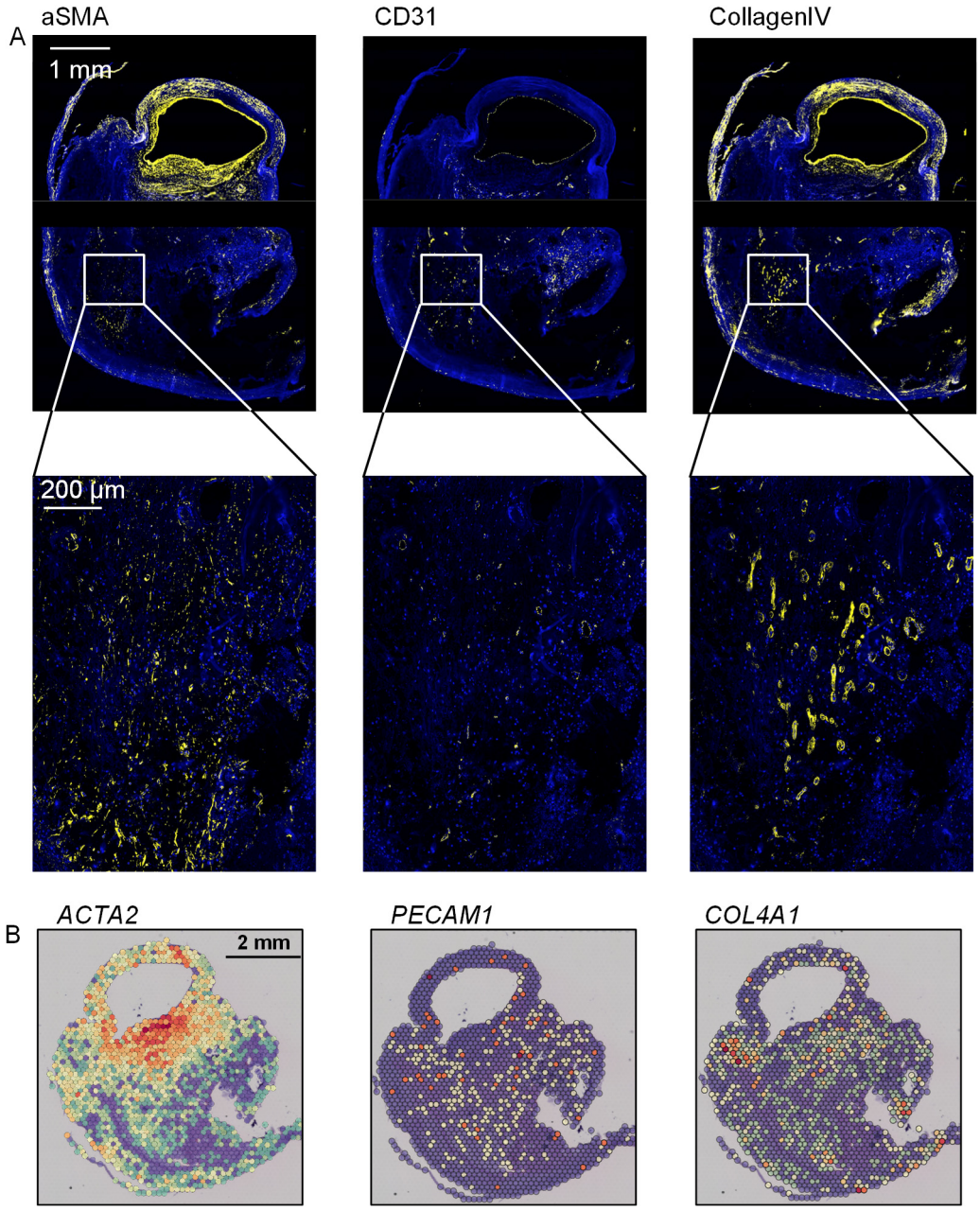

Supplementary Fig. 5. Spatial correspondence of the transcriptomic and proteomic signals for protein and gene pairs. Comparison of the A) proteomic and B) transcriptomic maps across the plaque for the following protein/gene pairs: αSMA protein and *ACTA2* gene, CD31 protein and *PECAM1* gene, and Collagen IV protein and *COL4A1* gene.

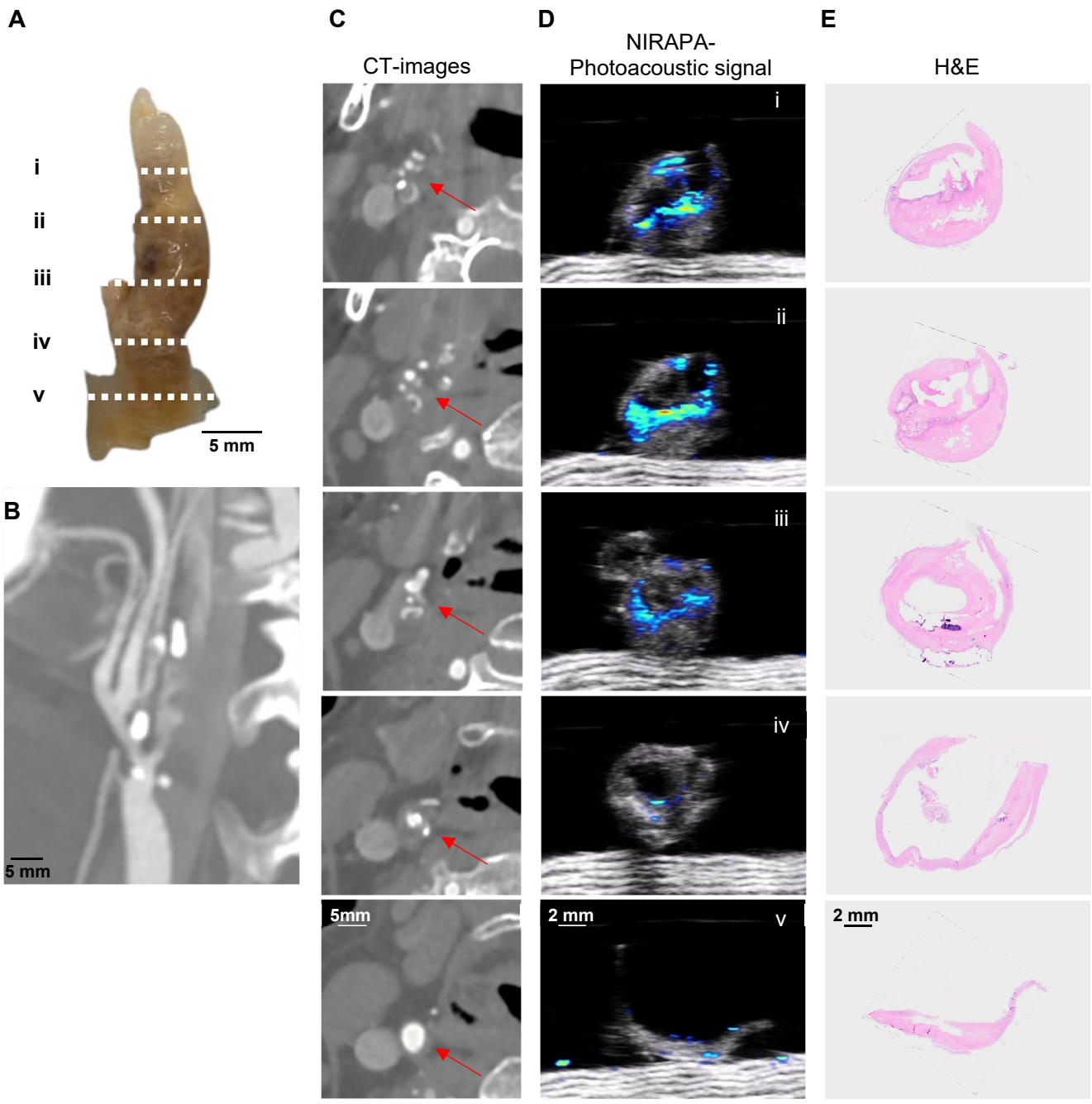

Supplementary Fig. 6. Comparison of contrast CT images with PAI images using the NIRAPA signal to detect vulnerable plaque compositions of a vulnerable carotid artery. A) Human carotid endarterectomy (CEA) specimen under white light. B) Corresponding longitudinal contrast computed tomography (CT) image shown underneath. The dashed lines on the longitudinal image represent the imaging locations of the axial images in columns C-E. C) Serial axial CT sections through the lesion of the carotid artery. Red arrows indicate location of stenosis. D) Serial axial PAI sections through the lesion of the carotid artery showing the NIRAPA signal. E) Corresponding H&E stains.

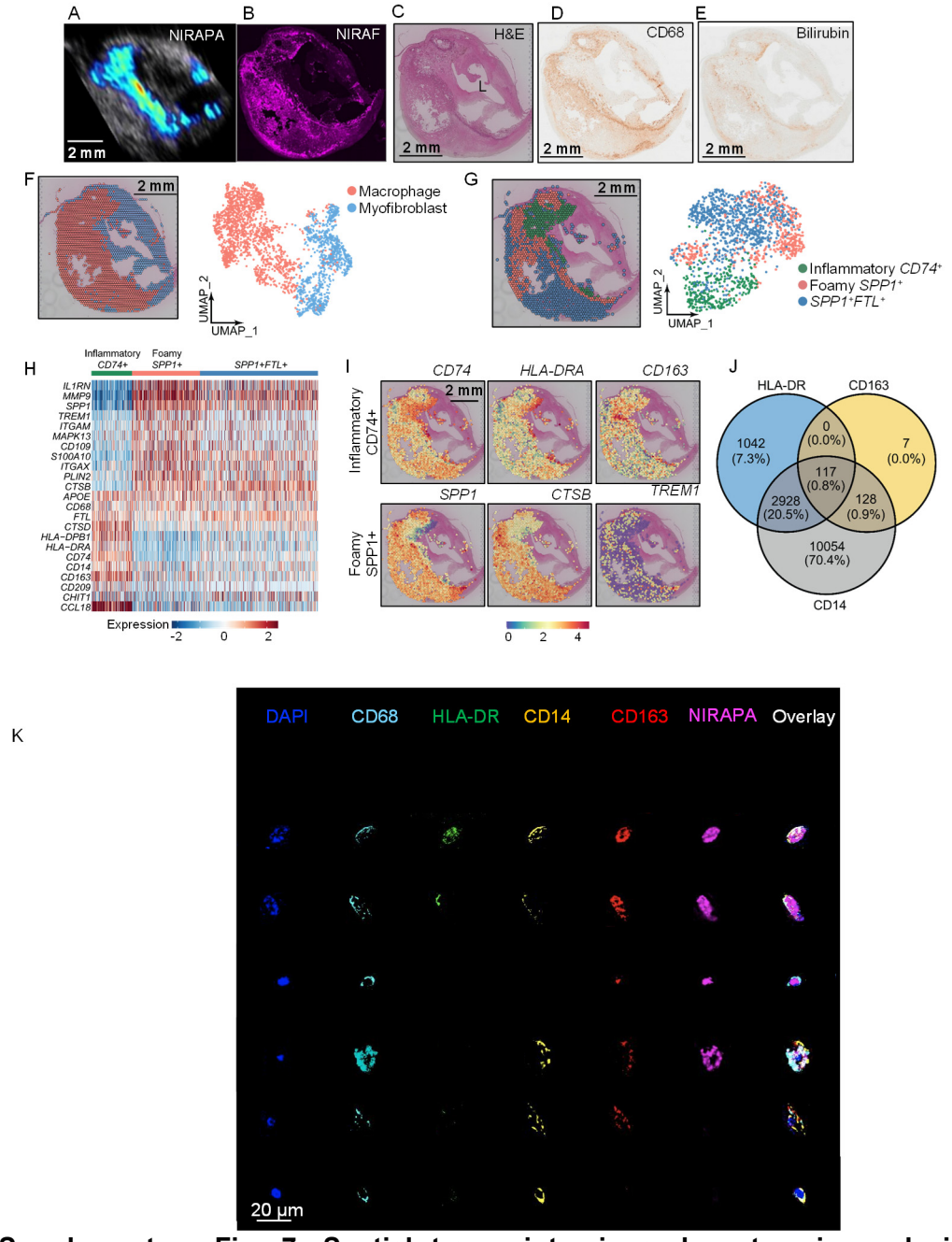

Supplementary Fig. 7. Spatial transcriptomic and proteomic analysis of vulnerable plaque delineates spatially-dependent macrophage populations. A-B) NIRAPA (A) and NIRAF (B) images of a carotid plaque cross section. C-E) Histological sections of the carotid endarterectomy (CEA) specimen stained with C) H&E, D) CD68 and E) bilirubin. F) Overlay and Uniform Manifold Approximation and Projection (UMAP) cluster projection of spatial transcriptomics on carotid plaque H&E. Based on their gene expression, clusters have been assigned to macrophage, myofibroblast and SMC intermediate cell types. G) Spatial deconvolution and UMAP of the macrophage cluster in CD74$^+$ and SPP1$^+$ regions and the spatial location on the H&E cross section. UMAP projection of macrophage high-resolution subtype clustering shows CD74$^+$, SPP1$^+$, and *SPP1*$^+$*FTL*$^+$ populations. H) Heatmap of macrophage-specific gene signatures that differentiate the *CD74*$^+$, *SPP1*$^+$, and *SPP1+FTL+* macrophage subpopulations. I) Key genes differentiating inflammatory (*CD74*$^+$) and foamy (*SPP1*$^+$) macrophages and their spatial location on the CEA specimen. J) Venn diagram of macrophage markers based on single-cell identification on CODEX. K) CODEX imaging of individual cells within the plaque shown in A-E to validate the source of the NIRAPA signal. P value cutoff is 0.005. Log_2FC cutoff is 2. L: Lumen.

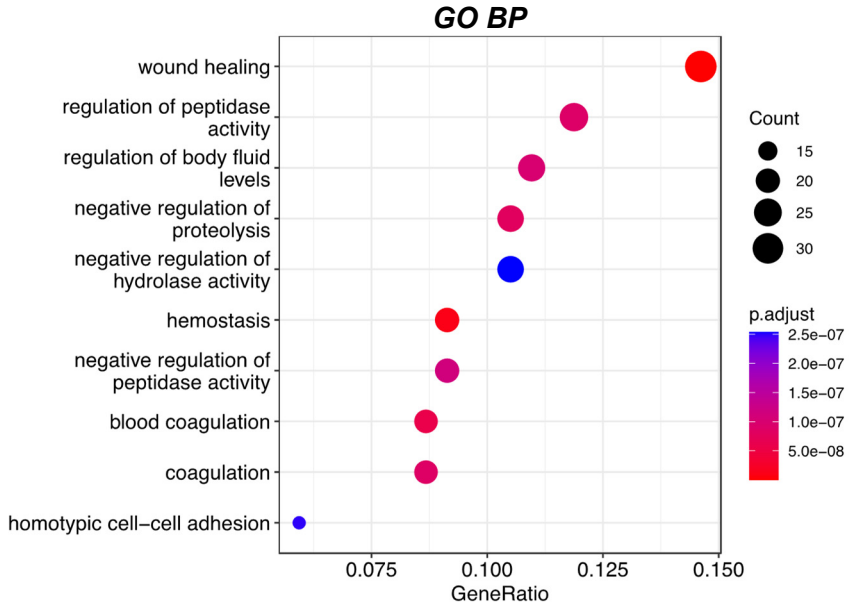

Supplementary Fig. 8. Enrichment results of vulnerable vs stable plaque. The differentially-expressed genes between vulnerable and stable plaque were determined by comparing mean gene expression values. Differentially-expressed genes with a fold change larger than 0 were then compared with gene ontology biological process (GO BP) database and the top 10 most significant biological processes based on adjusted p values were plotted.

Supplementary Table 1. Patient data and experimental plan

Case	Age	Sex	Symptoms	Fibrous Cap Thickness (Pathologist)	Ultrasound % stenosis	NIRAF	CD68, Bilirubin, Picrosirius Red, H&E, Masson's Trichrome, alpha SMA	Spatial Trans-criptomics and proteomics	CT/CTA
#1	75	M	yes	46	80-90%	X	X		None
#2	71	M	No	16	> 70%	X	X		None
#3	62	M	No	67	~60%	X	X		Short segment moderate stenosis (~ 60%) of the proximal left ICA
#4	72	M	yes	0	> 70%	X	X		None
#5	73	M	no	15	90-99%	X	X		None
#6	69	M	no	0	critical	X	X		None
#7	64	M	no	21	80-90%	X	X		None
#8	64	M	no	0	80-90%	X	X		Right w/ severe calcified and noncalcified atherosclerotic plaque of the right ICA just distal to the carotid bolb resulting in >90% stenosis. Additional focal outpouching consistent with deep plaque ulceration or focal pseudoaneurysm formation.
#9	66	F	yes	0	90%	X	X		Severe (90%) stenosis of the L ICA bulb.
#10	54	M	no	453	70-80%	X	X		None
#11	66	F	Yes	31	90%	X	X		None
#12	76	M	yes	70	95%	X	X		Bilateral cervical carotid artery stenoses, with calcifications, at the carotid bifurcation. L ICA 95%,
#13	62	F	yes	0	99%	X	X		None
#14	63	F	no	75	70-80%	X	X		70-80% of L proximal ICA ,
#15	76	M	yes	248	85%	X	X		Bilateral cervical carotid artery stenoses, with calcifications, at the carotid bifurcation. R ICA 85%.
#16	69	M	no	0	~95%	X	X		Bilateral carotide artery siphon stenosis
#17	79	M	yes	30	60%	X	X		60% stenosis at the right ICA origin
#18	80	M	no	774	-	X	X		Redemonstration of the severe arteriosclerotic irregularity of the bilaateral carotid

									siphons, right greater than left, with multifocal areas of severe stenosis.
#19	70	M	no	15	90-99%	X	X		None
#20	83	M	no	0	90-99%	X	X		Multifocal atherosclerotic disease with a short 6mm segment of occlusion of the right proximal internal carotid artery with distal reconstitution
#21	56	M	yes	0	60%	X	X		60% stenosis of the proximal R ICA
#22	84	M	yes	0	70-99%	X	X		Critical stenosis of R ICA
#23	58	M	yes	73	99%	X	X	X	Critical stenosis of the L ICA at the level of the distal bulb
#24	56	F	yes	0	99%	X	X	X	Critical stenosis of right ICA at level of carotid bulb.

Supplementary Table 2. CODEX Antibodies

Antigen	Clone	Company	Catalog	CODEX Oligo	Working Dilution	Exposure Time
ATM	EP1890Y	Akoya Biosciences	4250095		831:200	1/3 s
Bcl-2	EPR17509	Akoya Biosciences	4550089		851:100	1/6.5 s
Caveolin	D46G3	Akoya Biosciences	4550084		861:200	1/6.5 s
CD11c	118/A5	Akoya Biosciences	4550114		241:200	1/3 s
CD14	EPR3653	Akoya Biosciences	4450047		371:200	1/6.5 s
CD141	E7Y9P	Akoya Biosciences	4250097		871:200	1/6.5 s
CD163	EPR19518	Akoya Biosciences	4250079		691:200	1/3 s
CD20	L26	Akoya Biosciences	4150018		71:100	1/3 s
CD21	EP3093	Akoya Biosciences	4450027		321:100	1/3 s
CD3	EP449E	Akoya Biosciences	4550119		451:100	9/20 s
CD31	EP3095	Akoya Biosciences	4450017		11:100	1/4 s
CD34	QBEnd/10	Akoya Biosciences	4250057		251:200	1/3 s
CD38	E7Z8C	Akoya Biosciences	4250080		891:200	1/6.5 s
CD39	EPR20627	Akoya Biosciences	4250076		991:100	1/3 s
CD4	EPR6855	Akoya Biosciences	4550112		31:200	1/3 s
CD40	D8W3N	Akoya Biosciences	4550064		101:66	1/3 s
CD44	IM7	Akoya Biosciences	4450041		51:200	1/3 s
CD45	D9M81	Akoya Biosciences	4550089		211:200	1/3 s
CD45RO	UCHL1	Akoya Biosciences	4250023		171:200	1/3 s
CD66	ASL-32	Akoya Biosciences	4550001		161:800	1/3 s
CD68	KP1	Akoya Biosciences	4550113		151:200	1/3 s
CD79a	D1X5C	Akoya Biosciences	4450078		901:200	1/3 s
CD8	C8/144B	Akoya Biosciences	4250012		261:200	9/20 s
Collagen IV	EPR20966	Akoya Biosciences	4550122		421:200	1/6.5 s
E-Cadherin	4A2C7	Akoya Biosciences	4250021		141:200	1/3 s
EpCAM	D9S3P	Akoya Biosciences	4450088		911:200	1/3 s
ERa	SP1	Akoya Biosciences	4250074		841:200	1/3 s
FOXp3	236A/E7	Akoya Biosciences	4550071		311:50	1/3 s
Galectin-3	M3/38	Akoya Biosciences	4450034		351:200	1/6.5 s
GATA3	D13C9	Akoya Biosciences	4250085		491:100	1/3 s
GranzymeB	D6E9W	Akoya Biosciences	4250055		411:200	1/3 s
HLA-A	EP1395Y	Akoya Biosciences	4450046		41:200	1/3 s
HLA-DR	EPR3692	Akoya Biosciences	4550118		331:200	1/3 s
HLA-E	MEM-E/02	Akoya Biosciences	4250065		341:200	1/3 s
ICOS	D1K2T	Akoya Biosciences	4550117		541:200	1/3 s
IDO1	V1NC3IDO	Akoya Biosciences	4550123		271:200	1/3 s

IFNg	EPR21704	Akoya Biosciences	4250062	201:200	1/3 s
Keratin 8/18	C51	Akoya Biosciences	4550082	811:200	1/6.5 s
Ki67	B56	Akoya Biosciences	4250019	471:100	1/3 s
LAG3	EPR20261	Akoya Biosciences	4550058	551:50	1/3 s
MPO	E1E71	Akoya Biosciences	4250083	981:200	1/3 s
Pan-Cytokeratin	AE-1/AE-3	Akoya Biosciences	4150020	191:200	1/6.5 s
PCNA	PC10	Akoya Biosciences	4550124	361:200	1/6.5 s
PD-1	D4W2J	Akoya Biosciences	4550038	461:50	1/3 s
PD-L1	73-10	Akoya Biosciences	4550072	431:100	1/3 s
Podoplanin	NC-08	Akoya Biosciences	4250004	231:200	1/3 s
SMA	1A4	Akoya Biosciences	4450049	131:200	1/6.5 s
TIGIT	BLR047F	Akoya Biosciences	4250061	21:66	1/3 s
TP63	W15093A	Akoya Biosciences	4550081	931:800	1/3 s
Vimentin	O91D3	Akoya Biosciences	4450050	221:200	1/6.5 s
VISTA	D162G	Akoya Biosciences	4250063	401:66	1/3 s

Supplementary references

[1] L. Willemsen, M.P. de Winther, Macrophage subsets in atherosclerosis as defined by single-cell technologies, The Journal of pathology 250(5) (2020) 705-714.
[2] H. Pan, C. Xue, B.J. Auerbach, J. Fan, A.C. Bashore, J. Cui, D.Y. Yang, S.B. Trignano, W. Liu, J. Shi, Single-cell genomics reveals a novel cell state during smooth muscle cell phenotypic switching and potential therapeutic targets for atherosclerosis in mouse and human, Circulation 142(21) (2020) 2060-2075.
[3] T. Wu, E. Hu, S. Xu, M. Chen, P. Guo, Z. Dai, T. Feng, L. Zhou, W. Tang, L. Zhan, X. Fu, S. Liu, X. Bo, G. Yu, clusterProfiler 4.0: A universal enrichment tool for interpreting omics data, Innovation (Camb) 2(3) (2021) 100141.